Surface Defects on Plate-Shaped Silver Nanoparticles Contribute to Its Hazard Potential in a Fish Gill Cell Line and Zebrafish Embryos

Saji George,[†,‡] Sijie Lin,[‡] Zhaoxia Ji,[‡] Courtney R. Thomas,[§] LinJiang Li,[‡] Mathew Mecklenburg,[⊥] Huan Meng,[†,‡] Xiang Wang,[‡] Haiyuan Zhang,[‡] Tian Xia,[†,‡] J. Nathan Hohman,[§,#,▽] Shuo Lin,[∥] Jeffrey I. Zink,[§] Paul S. Weiss,[‡,§,#,▽] and André E. Nel[†,‡,▽,*]

[†]Department of Medicine, Division of NanoMedicine, [‡]Center for Environmental Implications of Nanotechnology, California NanoSystems Institute, [§]Department of Chemistry and Biochemistry, [⊥]Electron Microscopy Core Facility, California NanoSystems Institute, [∥]Department of Molecular, Cell, and Developmental Biology, [#]Department of Materials Science and Engineering, [▽]California NanoSystems Institute, University of California, Los Angeles, Los Angeles, California 90095, United States

ABSTRACT We investigated and compared nanosize Ag spheres, plates, and wires in a fish gill epithelial cell line (RT-W1) and in zebrafish embryos to understand the mechanism of toxicity of an engineered nanomaterial raising considerable environmental concern. While most of the Ag nanoparticles induced *N*-acetyl cysteine sensitive oxidative stress effects in RT-W1, Ag nanoplates were considerably more toxic than other particle shapes. Interestingly, while Ag ion shedding and bioavailability failed to comprehensively explain the high toxicity of the nanoplates, cellular injury required direct particle contact, resulting in cell membrane lysis in RT-W1 as well as red blood cells (RBC). Ag nanoplates were also considerably more toxic in zebrafish embryos in spite of their lesser ability to shed Ag into the exposure medium. To elucidate the "surface reactivity" of Ag nanoplates, high-resolution transmission electron microscopy was performed and demonstrated a high level of crystal defects (stacking faults and point defects) on the nanoplate surfaces. Surface coating with cysteine was used to passivate the surface defects and demonstrated a reduction of toxicity in RT-W1 cells, RBC, and zebrafish embryos. This study demonstrates the important role of crystal defects in contributing to Ag nanoparticle toxicity in addition to the established roles of Ag ion shedding by Ag nanoparticles. The excellent correlation between the *in vitro* and *in vivo* toxicological assessment illustrates the utility of using a fish cell line in parallel with zebrafish embryos to perform a predictive environmental toxicological paradigm.

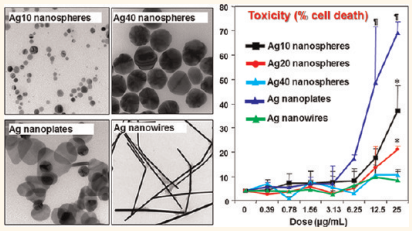

KEYWORDS: silver · nanomaterial · crystal defect · shape · surface reactivity · nanosphere · nanoplate · nanowire · RT-W1 · zebrafish · predictive toxicology

Safe implementation of nanotechnology requires an in-depth understanding of the properties of engineered nanomaterials (ENMs) that could lead to hazardous effects in humans and the environment. More than 30% of nanoenabled consumer products currently include Ag nanoparticles that could be released from these materials to generate exposures in humans and the environment.[1−4] This exposure potential is generating a considerable concern about the potential adverse impact of Ag nanoparticles in humans and the environment. Thus, while Ag nanoparticles appear to be relatively toxic to bacteria,[1] algae,[2] daphnia,[5,6] and a variety of fish species, several studies (including our own) have shown little toxicity in mammalian systems.[7−9] The apparently high level of tolerance in humans has allowed the implementation of metallic silver and various silver salts as treatment options for infectious disease long before the advent of antibiotics.

Ag nanoparticles have been shown to be a source of ionic silver because of their dissolution in a biological environment.[4,10] Consequently, the shedding of silver ions in the exposure medium and possibly in proximity to the nanobio interface has been attributed as the primary mechanism of Ag nanoparticle toxicity in aquatic lifeforms. However, this may not be the only characteristic that is of importance in Ag nanoparticle toxicity because the catalyst industry is introducing alternatively shaped metallic nanoparticles with increased surface reactivity. It has also been demonstrated that nanoparticle shape may impact biological outcome as a result of differences in the cellular uptake, biocompatibility, and organ retention.[11,12] For instance, in a recent study conducted in zebrafish embryos, dendrimer-shaped nickel nanoparticles were shown to exhibit higher toxicity than spherical nanoparticles.[13] The shape effect of Ag nanoparticles has been observed in bacteria,[1,12] with

* Address correspondence to anel@mednet.ucla.edu.

Received for review December 1, 2011 and accepted April 6, 2012.

Published online April 06, 2012
10.1021/nn204671v

Ag nanoplates showing a higher degree of toxicity. However, to our knowledge, a systematic investigation into the shape-dependent toxicity of Ag nanoparticles has not been carried out in eukaryotes to date. Moreover, while alternate mechanisms of Ag nanoparticle toxicity have been suggested,[14] current models of aquatic toxicology do not include a systematic dissection of toxicity in an environmentally relevant eukaryotic cell, which would be preferred over the use of mammalian cell lines for elucidating mechanisms of toxicity in relevance to aquatic lifeforms.

The fish gill is a vital organ for gas exchange, osmotic regulation, acid−base homeostasis, nitrogenous waste excretion, and endocrine regulation.[15] The direct exposure of the gill to the external environment establishes this organ as one of the primary targets for toxicological injury by heavy metals, pesticides, acidifiers, nitrogenous compounds, *etc*. Several reports suggest the ability of ENMs to target[16] and to induce morphological abnormalities in the epithelial layer of the gill in parallel with pathophysiological changes that impact osmoregulation.[17,18] In fact, the action of Ag ions on the Na^+/K^+ pump in the gill epithelium reduces active Na^+ and Cl^- uptake, leading to dysregulation of osmotic balance, cardiac failure, and death of the fish.[19] Premised on the importance of gill physiology, primary cultures of fish gill cells have been used successfully for toxicological testing.[20] Such systems could also be implemented to study ENM toxicity and to make predictions of what could happen *in vivo*.

Here, we report the use of a rainbow trout gill epithelial cell line (RT-W1) to explore the mechanism of toxicity of different Ag nanoparticle shapes as well as a comparative toxicological analysis in zebrafish embryos. We demonstrate that Ag nanoplates show a higher level of toxicity compared to nanospheres and nanowires in spite of the lower rates of dissolution and bioavailability of this material shape. Further investigation revealed that the higher toxicological potential of Ag nanoplates- to a considerable extent- is based on their surface reactivity, which can be mitigated by surface passivation with cysteine. In addition, we demonstrated that the gill epithelial cell line could be used for *in vitro* hazard ranking to predict the outcomes in intact zebrafish embryos.

RESULTS

Physicochemical Characterization of Ag Nanoparticles. We used a series of polyvinylpyrrolidone- (PVP) coated Ag nanoparticles that include nanospheres of different sizes (10, 20, and 40 nm), nanoplates, and nanowires. Among the Ag nanospheres, those with diameters of 20 and 40 nm showed a homogeneous size distribution while 10-nm spheres showed a size variation of 7−15 nm (Figure 1a). For Ag nanoplates, the shapes varied from circular to triangular but exhibiting edges

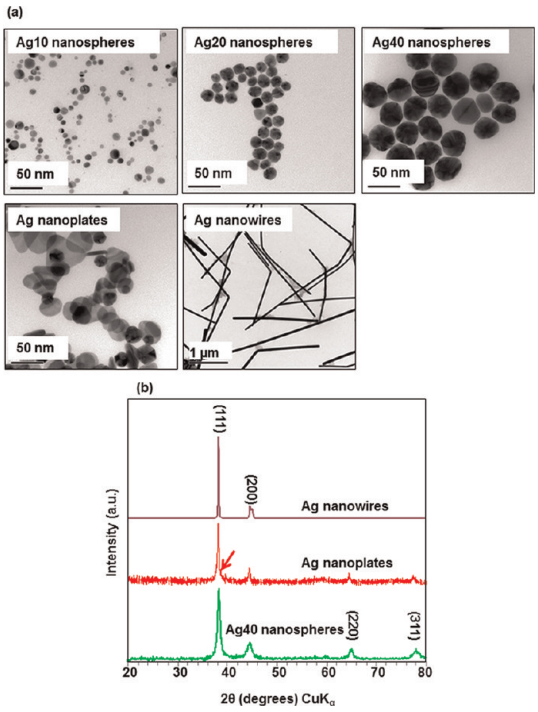

Figure 1. Physicochemical characterization of Ag nanoparticles. (a) TEM images of the Ag nanoparticles used in this study. The images were taken with a JEOL 1200 EX TEM microscope with an accelerating voltage of 80 kV. The images demonstrated that all the nanoparticles exhibit well-defined single crystalline structures. (b) XRD pattern of Ag40 nanospheres, Ag nanoplates, and Ag nanowires. The XRD patterns were collected with a step size of 0.02° and counting time of 0.5 s per step over a range of 20−80° 2θ. The XRD analyses of the Ag nanospheres, Ag nanoplates, and Ag nanowires demonstrate high crystallinity. All peaks could be indexed to the fcc phase of silver, indicating a single phase in each product.

(Figure 1a). While Ag nanowires showed a consistent diameter of 60 nm, they varied from 5 to 20 μm in length (Figure 1a). Other than size and shape, another distinguishing feature of the individual Ag nanoparticle types was the difference in plasmonic resonance as a result of the shape differences (Supplementary Figure S1, Supporting Information). Thus, while spherical Ag nanoparticles showed a single plasmonic resonance peak at 390−410 nm, nanoplates showed peaks at 330, 410, and 630 nm, confirming their anisotropy. The X-ray diffraction (XRD) patterns of the Ag nanoparticles confirm their crystalline structure, with characteristic diffraction peaks originating from {111}, {200}, and {311} lattice planes (Figure 1b). Although the XRD patterns of the Ag nanospheres and nanoplates were similar, the Ag nanoplates showed shoulder peaks at {111}, suggesting the presence of structural defects.[21] In contrast, Ag nanowires showed predominantly diffraction intensity from the {111} and {200} lattice planes, with negligible diffraction from {311}.

Because the study of the biological effects of Ag nanoparticles requires experimentation under exposure conditions that lead to particle agglomeration,

TABLE 1. Hydrodynamic Diameter of Ag Nanoparticles in Water and Exposure Media[a]

			medium alone			media supplemented with alginate	
NPs	primary particle size (nm)[b]	number of particles/mg[b]	water	Holtfreter's medium	L-15	Holtfreter's medium	L-15
Ag10 nanospheres	10	4×10^{14}	26.4	297.7	1802	174	310.3
Ag20 nanospheres	20	2.1×10^{13}	45.9	107.4	1763.3	37	350.3
Ag40 nanospheres	40	2.5×10^{12}	61.2	89.5	1943.3	40	211.6
Ag nanoplates	45×10	1.13×10^{13}	41.7	50.1	1564	45	291.6
Ag nanowires	20000×65	2.09×10^{10}	548	1256	2134.3	764	833.6

[a] The average hydrodynamic diameter of Ag nanoparticles suspended in water and exposure media was assessed in the absence and presence of alginate supplementation. The working concentration of nanoparticle suspensions were prepared by aliquoting 25 μL of the original nanoparticle suspension (stock concentration of 1 mg/mL) to 1 mL of water or exposure media. These nanoparticle suspensions were sonicated using a probe sonicator (15 min, 30 W) before measuring their hydrodynamic size using DLS (Dynapro, Wyatt Technologies, Santa Barbara, CA). While the PVP-coated Ag nanoparticles disperse well in water, they tended to undergo agglomeration in the exposure media. Supplementation of these media with alginate decreased the average size of the agglomerates. The apparent high and somewhat inaccurate hydrodynamic diameter of Ag nanowires is due to their long aspect ratio. [b] data from supplier.

TABLE 2. Zeta Potential of Ag Nanoparticles in Water and Exposure Media[a]

	medium alone			media supplemented with alginate	
NPs	water	Holtfreter's medium	L-15	Holtfreter's medium	L-15
Ag10 nanospheres	−34 (±1.9)	−1.6 (±3.43)	−12.9 ± 1.22	−11.4 (±1.8)	−20 (±1.3)
Ag20 nanospheres	−51.7 (±2.4)	−5.6 (±2.1)	−6.5 ± 2.03	−17.9 (±3.5)	−16.9 (±1.9)
Ag40 nanospheres	−35.4 (±1.3)	−4.8 (±1.19)	−11.3 ± 0.69	−16.9 (±1.6)	−20 (±3.2)
Ag nanoplates	−36.7 (±0.8)	−12.8 (±2.3)	−17.1 ± 3.54	−19.5 (±2.3)	−22.9 (±7.1)
Ag nanowires	−27.3 (±1.0)	−4.5 (±1.33)	−7.8 ± 2.47	−6.3 (±3.2)	−17.8 (±4.1)

[a] The preparations of the nanoparticle suspensions were similar to the details provided in Table 1. Zeta potential was assessed using Zeta potential analyser (ZetaPALS, Brookhaven Instruments, Holtsville, NY). All of the Ag nanoparticles showed negative surface charge in water, which was decreased in the exposure media prior to the addition of alginate. The increase in net negative surface charge upon the addition of alginate could play a role in the improved particle dispersion in L-15 and Holtfreter's medium.

we characterized the size, state of agglomeration, and surface charge of all the materials in water as well as cell culture (L-15 medium) and Holtfreter's medium supplemented with alginate (Table 1). Alginate is an environmentally relevant dispersing agent that helps to stabilize nanoparticles in aqueous suspension.[9] While the dispersal of the Ag nanospheres and nanoplates were improved by the addition of alginate, the average hydrodynamic diameters of the Ag nanowires in Holtfreter's and L-15 media were not changed to similar degrees (Table 1). The surface charge of these materials, as determined by measurement of their zeta-potential, showed that the addition of alginate increased their negative surface charge, which could be contributing to the improved dispersion in the growth media (Table 2).

Comparative Differences in the Toxicity of Ag Nanoparticles in RT-W1 Cells. A culture of the rainbow trout gill fish cell line, RT-W1, was established in L-15 medium for the performance of high-throughput toxicological screening in our automated screening facility in the California NanoSystems Institute (CNSI). Following the addition of the various Ag nanoparticles over a wide dose range of 0.356−25 μg/mL to 384 well plates at room temperature, a cocktail of fluorescent dyes was used to assess cell viability and intracellular superoxide production. In wells receiving propidium iodide (PI) to assess cell membrane damage, Ag nanoplates induced significant cell death even at the lowest dose, while the nanospheres (Ag10, Ag20, and Ag40) induced cytotoxicity at the highest doses and Ag nanowires did not (Figure 2a). Thus, at the highest dose tested (25 μg/mL), Ag nanoplates induced the death of ~70% of cells in the population while Ag10, Ag20, and Ag40 induced cytotoxicity of 37, 21, and 10% of cells, respectively. When cytotoxicity was expressed according to a surface area dose metric, the dominant effect of the Ag nanoplates was maintained while the differences between the spherical nanoparticles disappeared as a result of correcting for the differences in surface area (Figure 2b).

Our earlier studies in mammalian cells have shown that diverse types of nanomaterials are capable of inducing oxidative stress as the mechanism of biological injury and therefore potentially useful for ranking ENM toxicity based on redox potential.[9,22,23] Since Ag nanomaterials are capable of oxygen radical generation, we studied the possibility that the RT-W1 toxicity is oxidative stress related. Therefore, we treated RT-W1 cells with *N*-acetylcysteine (NAC) prior to exposing them to Ag nanoparticles. *N*-acetylcysteine is a glutathione precursor as well as a quencher of oxygen free radicals.[24] Preincubation with NAC was associated with a 6-fold reduction in the percentage of cells exhibiting

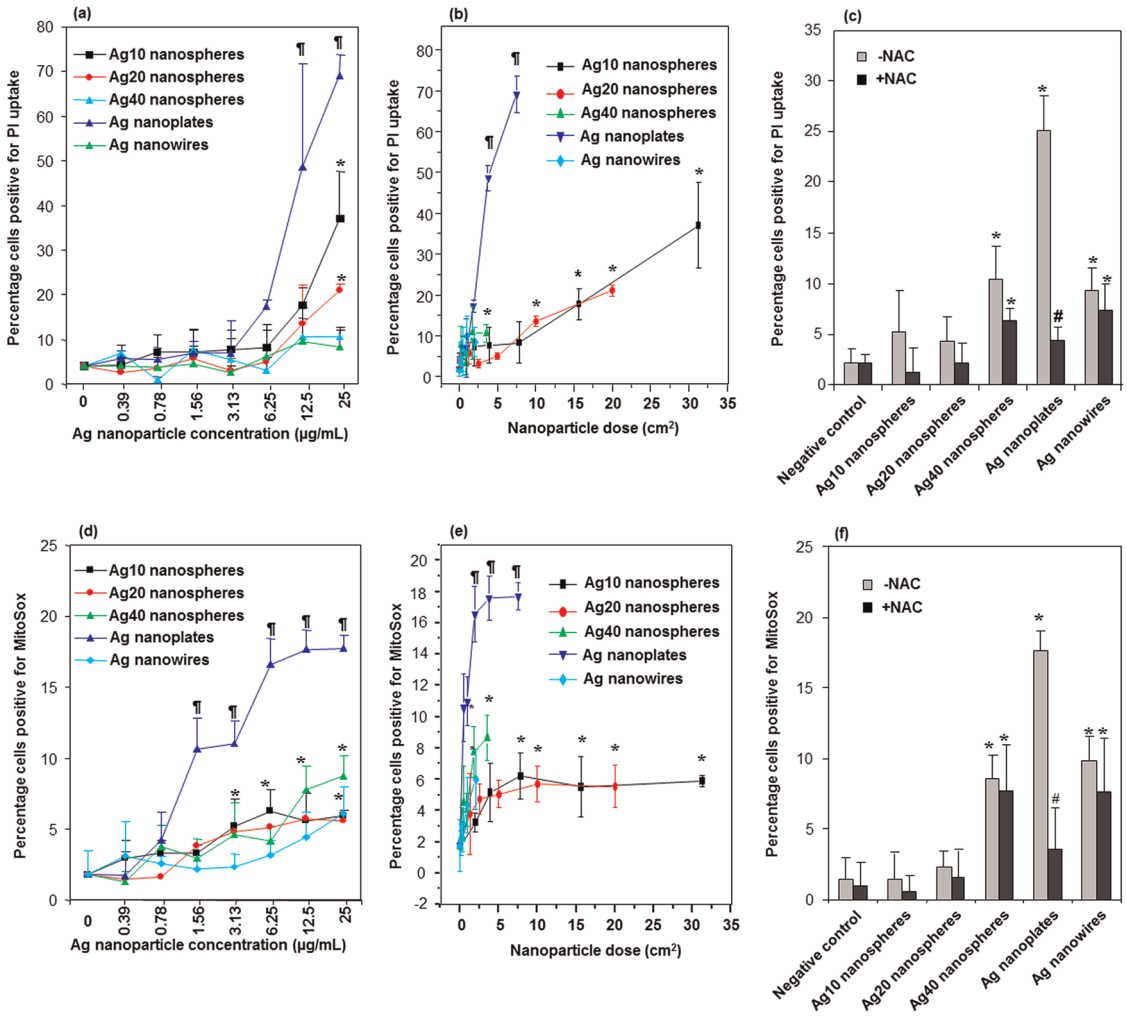

Figure 2. Cytotoxicity in RT-W1 cells treated with Ag nanoparticles. (a) RT-W1 cells grown in 384 well plates were exposed to incremental concentrations (0−25 μg/mL) of Ag nanoparticles at room temperature for 24 h. Each well received 25 μL of a dye cocktail that included Hoechst 33342 (1 μM) and PI (5 μM) to detect the total number of nuclei as well as assess compromised cell membrane integrity. The numbers of PI-positive cells were scored by automated epifluorescence microscopy and expressed as a percentage of the total cell number (Hoechst-positive cells). This panel depicts the dose−response relationship of the different Ag nanoparticles using a mass dose metric. (b) Expression of the same data as shown in a in terms of surface area dose, in which the specific surface area was calculated according to the number of particles present in 1 mL of medium. As for the mass-dose calculations, Ag nanoplates dominated other Ag nanoparticles in terms of toxicity while Ag nanowires had the least impact. (c) RT-W1 cells treated with 1 mM NAC for 24 h before exposure to Ag nanoparticles (10 μg/mL) and assayed for PI uptake as described above. (d) RT-W1 cells grown in 384 well plates were treated with Ag nanoparticles as detailed above. Twenty-five microliters of a dye cocktail, including Hoechst 33342 (1 μM) and MitoSox red (5 μM), was added to each well in the multiwall plate to detect cellular nuclei and to assess mitochondrial superoxide production, respectively. The percentage of cells positive for mitochondrial superoxide was measured as detailed in materials and methods. (e) Expression of the same data in d in terms of surface area dose, in which the specific surface area was calculated according to the number of particles present in 1 mL of medium. The data demonstrate that Ag nanoplates dominated in their ability to generate superoxide, as compared to other shapes. (f) RT-W1 cells prior treated with 1 mM NAC for 24 h were subsequently treated with a Ag nanoparticle dose of 10 μg/mL and assayed for superoxide production. While NAC pretreatment significantly reduced superoxide generation by several of nanoparticles, the inhibition was most significant for Ag nanoplates. All of the above experiments were repeated three times with triplicates in each group. * statistically different from control ($p < 0.05$). ¶ The values for Ag nanoplates are statistically significant from other Ag nanoparticle types ($p \leq 0.05$), and # significant decrease in the response due to NAC treatment ($p \leq 0.001$). Error bars represent the standard deviation from average values.

cytotoxicity in response to Ag nanoplates exposure (Figure 2c). Although, NAC also decreased the toxicity of Ag40 nanospheres and Ag nanowires, the magnitude of decline in the level of injury was not as dramatic as for the Ag nanoplates, demonstrating the importance of oxidative stress for this material. In order to assess oxygen radical production at the cellular level more directly, we also used MitoSox Red to assess superoxide radical production in RT-W1 cells.[9] While the percentage of cells scoring positive for mitochondrial superoxide production showed a dose-dependent increase for most Ag nanoparticles, the steep dose−response relationships of the Ag nanoplates outstripped those of the other materials and were in agreement with their more robust effect on

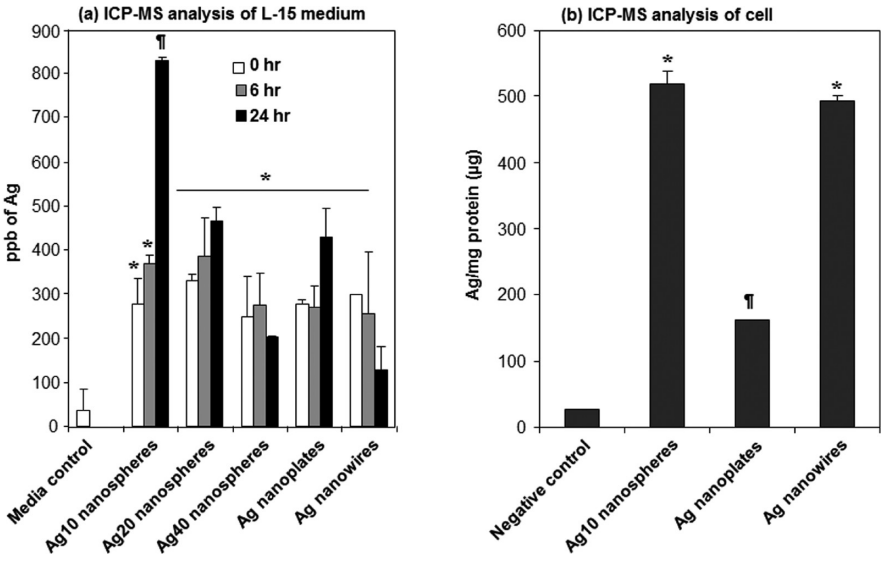

Figure 3. ICP-MS analysis to study elemental Ag release from the nanoparticles into L-15 medium or for the assessment of total Ag content in nanoparticle-treated cells. (a) Five μL of Ag nanoparticle stock solution (1 mg/mL in water) was added to 1 mL of L-15 medium supplemented with 100 ppm of alginic acid before sonication. One hundred microliters of each particle suspension was dispersed into the wells of a 96 well plate and incubated at room temperature. Aliquots were withdrawn at 0, 6, and 24 h, ultracentrifuged, and 50 μL of each supernatant used for acid hydrolysis and ICP-MS analysis. Among the particles tested, Ag10 showed the highest level of Ag shedding. (b) ICP-MS analysis to assess the total Ag content of RT-W1 cells. The cells were cultured in 6 well plates. Each well received 5 mL of a 5 μg/mL Ag nanoparticles suspension. After 24 h of incubation at room temperature, the incubation medium was removed, cells were rinsed three times with PBS, scraped from the well bottoms, and homogenated in PBS. One hundred microliters of each cellular homogenate was taken for acid hydrolysis and ICP-MS analysis. The average values of three replicates were used to calculate the ppb of Ag per mg of cellular protein. The total Ag content of Ag-nanoplate-treated cells was significantly lower than cells treated with other Ag nanoparticles. * Statistically significant difference from untreated cells ($p \leq 0.05$). ¶ the values for Ag nanoplates are statistically significant from other Ag nanoparticle types ($p \leq 0.05$).

cytotoxicity (Figure 2d). Thus, Ag nanoplates triggered significantly more superoxide production, even at the lowest dose tested. Even more dramatic differences were seen when the MitoSox Red data were expressed according to a surface area dose metric (Figure 2e). This suggests the importance of surface reactivity in the toxicological outcome. NAC also suppressed superoxide production by Ag40 nanospheres, Ag nanoplates, and Ag nanowires (Figure 2f). However, the antioxidant protective effect was most noticeable for Ag nanoplates, leading to a 5-fold reduction in superoxide production (Figure 2f).

Dissolution and release of Ag ions have frequently been reported as the primary mechanism of Ag-nanoparticle toxicity in aquatic life forms.[8,9] Therefore, we used inductively coupled plasma mass spectrometry (ICP-MS) to quantify Ag metal ion shedding in L-15 medium as well as measuring the total Ag content in cells treated with different Ag nanoparticles. The data show that shedding of free Ag is highest for Ag10 nanospheres where the concentration of dissolved Ag species increased significantly from 290 to 850 ppb over a 24 h observation period (Figure 3a). In contrast, Ag release from the other Ag nanoparticles (Ag20, Ag40, Ag nanoplates, and Ag nanowires) was insignificant compared to Ag10 (Figure 3a). When comparing total cellular Ag content by ICP-MS, which detects particle-associated as well as free silver ion, the silver content in the homogenates was found to be 519, 162, and 493 μg Ag per mg cellular protein, respectively, for Ag10, Ag nanoplates, and Ag nanowires (Figure 3b). This demonstrates that the bioavailability of Ag is significantly lower in Ag-nanoplate-treated cells compared to cells exposed to Ag10 nanospheres and Ag nanowires. All considered, these results suggest that the higher cytotoxicity of Ag nanoplates is not well correlated to Ag bioavailability and uptake, suggesting that this material may introduce a novel form of toxicity.

To relate this finding to the cellular uptake and bioprocessing of Ag nanoparticles as determined by transmission electron microscopy (TEM), RT-W1 cells were incubated with the different particle types for 24 h. Visualization of the micrographs showed poor cellular uptake of intact Ag nanoparticles, with the exception of nanowires that could be detected intracellularly and protruding from the surface membrane (Supporting Information, Figure S2). In contrast, Ag nanoplates and nanospheres were difficult to locate intracellularly, but were associated with the detection of electron-dense material at the ruffled surface membrane (Figure S2). However, Ag nanoplates did elicit prominent morphological changes in the nucleus and cellular interior that are consistent with cytotoxicity and cell death, including the formation of large vacuoles containing concentric layers of damaged lipid membranes (Figure S2). Taken together, this suggests

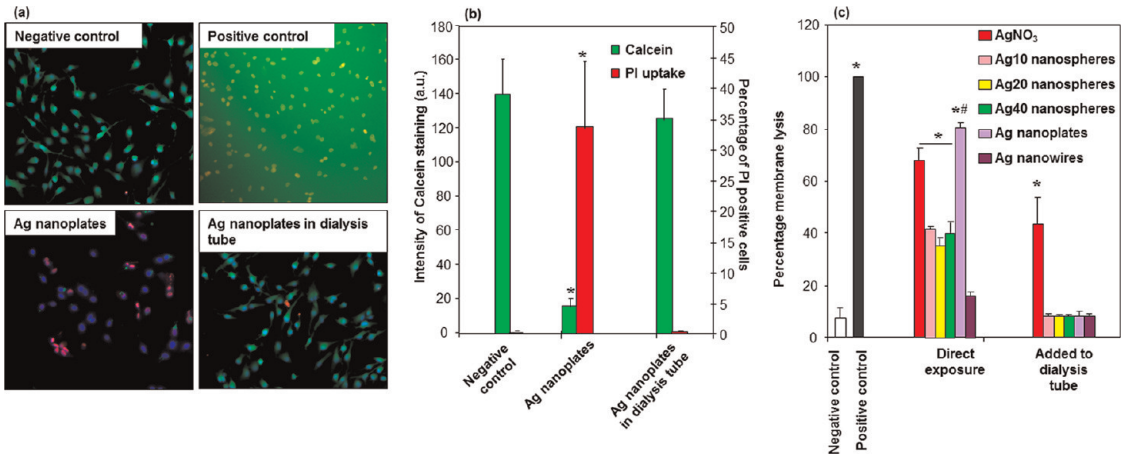

Figure 4. Fluorescence microscopy to demonstrate differences in the membranolytic activity of Ag nanoplates during direct and indirect contact with RT-W1 cells. (a) RT-W1 cells grown in 24-well plates received 10 μL/mL of a Ag-nanoplate suspension added directly to the well or introduced in a dialysis bag that was immersed in the cell culture medium. Following incubation for 24 h, the culture medium was removed and the wells received 500 μL of PBS that contained a dye mixture of Hoechst 33342, Calcein-AM, and Propidium iodide (PI). After incubation for a further 30 min, the cells were imaged under a fluorescence microscope. Healthy unexposed cells demonstrated green fluorescence staining by calcein in the cytosol, which partially obscures the Hoechst-stained (blue) nuclei. However, following direct contact with Ag nanoplate, disruption of the surface membrane catalyzed calcein escape and PI uptake into a few cells. In contrast, similar changes were not seen when the Ag nanoplate were introduced in a dialysis bag. Cellular lysis with Triton X-100 served as the positive control, while untreated cells served as the negative control. (b) Change in fluorescence intensity was analyzed using Image J software to express quantitatively the number of cells showing decreased calcein content and increased PI uptake in the nucleus. Thus, while direct addition of Ag nanoplates resulted in ~100-fold increase in PI uptake and ~10-fold decrease in calcein fluorescence intensity, separation of the nanoplate considerably reduced the membranolytic and cytotoxic effects. (c) Measurement of erythrocyte lysis with Ag nanoparticles and $AgNO_3$ added directly to or physically segregated from the RBC. Heparinized mouse RBC were treated with 10 μg/mL Ag nanoparticles or $AgNO_3$ (2.5 ppm) for 4 h. The samples were centrifuged and the hemoglobin absorbance of the supernatants measured at 540 nm in a microplate reader. Triton X-100 (5%), leading to 100% cell lysis, was used as the positive control to normalize all the values. While direct contact with Ag nanoparticles or $AgNO_3$ induced RBC lysis, the effect was significantly higher for Ag nanoplates. However, when the Ag nanoparticles were introduced in dialysis tubing, the lytic effect was dramatically reduced. $AgNO_3$ leaching from the dialysis bag could also induce RBC lysis. Experiments were repeated three times, using triplicates in each group. * Statistically significant from control ($p < 0.05$). # statistically significant differences between Ag nanoplates and other nanoparticle types ($p \leq 0.05$). Error bars represent the standard deviations from average values.

that the high Ag nanoplate toxicity is mediated by a mechanism other than nanoparticle uptake into the cells or dissolution. One possible explanation is direct Ag nanoplate contact with the cell membrane, leading to membranolytic injury.

Direct Physical Contact and Membrane Damage by Ag Nanoplates as a Mechanistic Explanation for the Differential Cytotoxicity of This Material. To test if direct physical contact is a prerequisite for cellular injury, we exposed RT-W1 cells to Ag nanoplates introduced directly to the medium or contained in a semipermeable dialysis membrane immersed in the culture medium. Prior to the test, cells were exposed to a dye cocktail that included Hoechst 33342, Calcein-AM, and Propidium iodide (PI) to quantify the number of nuclei, cells with surface membrane damage (Calcein escape), and dying cells, respectively (Figure 4a). Thus, in healthy nonparticle-exposed cells (negative control), the fluorescent intracellular calcein could be seen to leach from the cell during direct exposure to Ag nanoplates, leaving behind Hoechst-stained nuclei only or occasionally resulting in dead cells with positive nuclear staining for PI (Figure 4a). Triton X-100 totally disrupted cell morphology and calcein release (positive control). In contrast, the introduction of the Ag nanoplates in a dialysis membrane had no effect on membrane permeability with occasional cells demonstrating increased PI uptake (Figure 4a). Quantitative assessment of the data by Image J software further confirmed that the change in calcein and PI fluorescence intensities showed statistically significant differences between directly and indirectly exposed cells (Figure 4b). These results demonstrate that direct cellular access is a prerequisite for the induction of cytotoxicity and strengthens the notion that the surface reactivity of Ag nanoplates plays a major role in the membrane damage.

To compare the membranolytic effect of Ag nanoplates more directly with other Ag nanoparticles, we also used a red blood cell (RBC) lysis assay that serves as a sensitive screening tool to assess the surface reactivity of toxic particles.[25,26] All Ag nanoparticles with the exception of Ag nanowires induced erythrocyte lysis (Figure 4c). Compared to the lesser effects of Ag10, Ag20, and Ag40 nanospheres, direct Ag nanoplate exposure induced the lysis of ~80% RBC (Figure 4c). While nanospheres also induced dose-dependent RBC lysis, the effect of Ag10 was more robust (Figure S3, Supporting Information). When introduced in dialysis

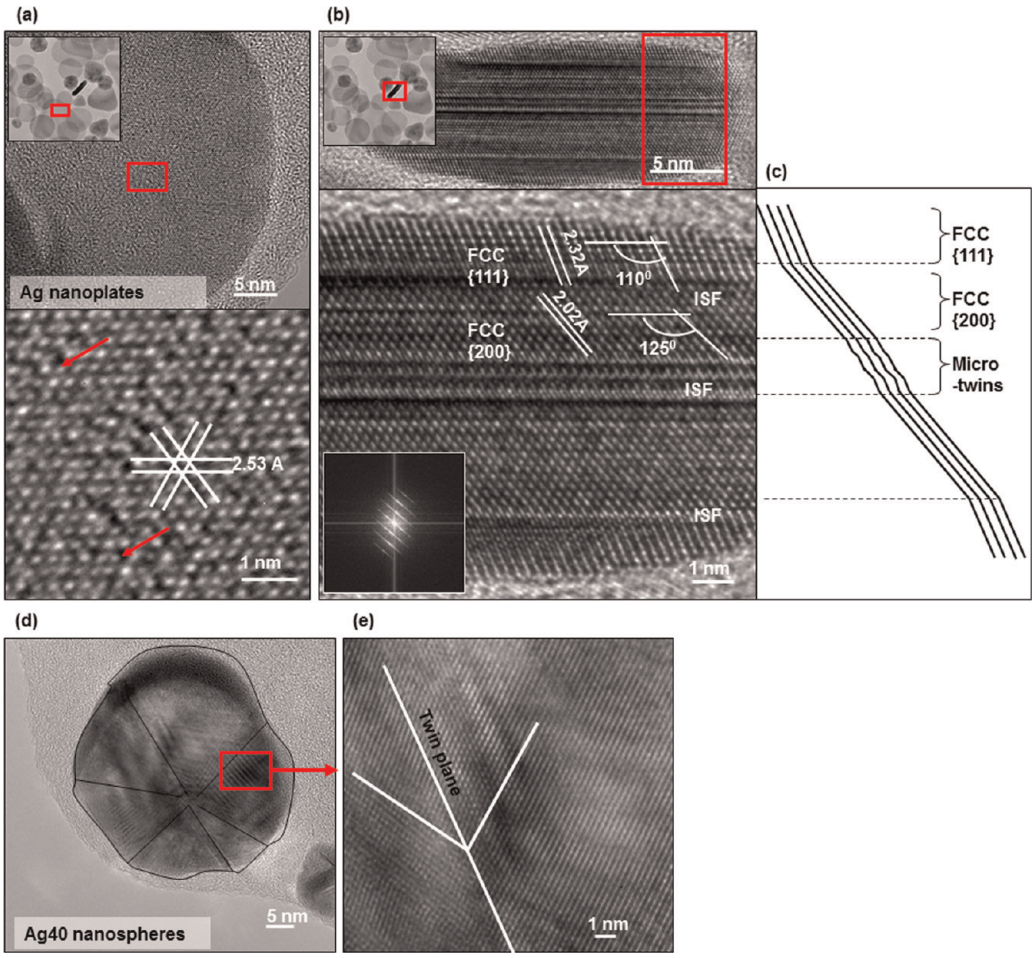

Figure 5. High-resolution TEM of Ag nanoparticles revealing the crystal defects in Ag nanoplates. (a) TEM image of a flat-lying Ag nanoplate. The higher magnification at the bottom left shows the 6-fold symmetry and the 2.53 Å spacing between the lattice fringes. (b) High-resolution image of a vertically oriented {110} plane (i.e., along the plane of the image) of a Ag nanoplate to show its structural defects. The image at the lower bottom provides the analysis of the internal plate structure. The inset at bottom right is a Fourier transform of the entire image. (c) Series of intrinsic stacking fault is evident in the schematic image of lattice image showing domain boundaries and microtwins. (d) HRTEM image of a Ag nanosphere (40 nm) showing the multiple domains. (e) High magnification showing the twin plane at the boundary of the domains. The crystal defects seen in Ag nanoplates are absent from Ag nanospheres.

tubing, none of the materials were capable of inducing erythrocyte lysis (Figure 4c), confirming the importance of direct contact with the surface membrane.

High Levels of Crystal Defects on the Ag Nanoplate Surfaces. Since crystal faces exposed to the environment could contribute to ENM surface reactivity,[25] high-resolution transmission electron microscopy (HRTEM) was used to explore crystal defects in Ag nanoplates, with Ag40 nanospheres serving as a comparative control (Figure 5). The TEM image of a typical flat-lying Ag nanoplate in Figure 5a demonstrates that this material is comprised of single crystals with a 6-fold axis of symmetry (lower panel). The dark spots (red arrow) at the planar surface of the nanoplate represent point defects that are introduced by missing atoms in the unitary crystal structure. Figure 5b shows the HRTEM image of a vertically oriented {110} plane, which upon more detailed analysis of the internal structure (lower panel) demonstrates a lattice spacing of 2.32 Å in the top layer and 2.03 Å in the latter. This is characteristic of a material with {111} and {200} fcc features, respectively. Most importantly, we observed a series of intrinsic stacking faults as shown in the schematic lattice image (Figure 5c). These stacking faults, which were present in almost all of the nanoplates, originate from the irregularity of the stacking planes of the atoms in the crystal lattice. A representative series of HRTEM images showing the prevalence of crystal defects is shown in Figure S4 (Supporting Information). Unlike the structure of the nanoplates, the Ag40 nanospheres showed multiple crystal domains (Figure 5d), including the presence of twin planes that form at the boundaries between different crystal domains (Figure 5e). However, the numbers of crystal defects in these spheres were comparatively lower than observed for the Ag nanoplates.

Surface Coating with Cysteine Ameliorated the Toxic Potential of Ag Nanoplates. Crystal defects have been reported to increase the chemical reactivity of Ag nanoparticles

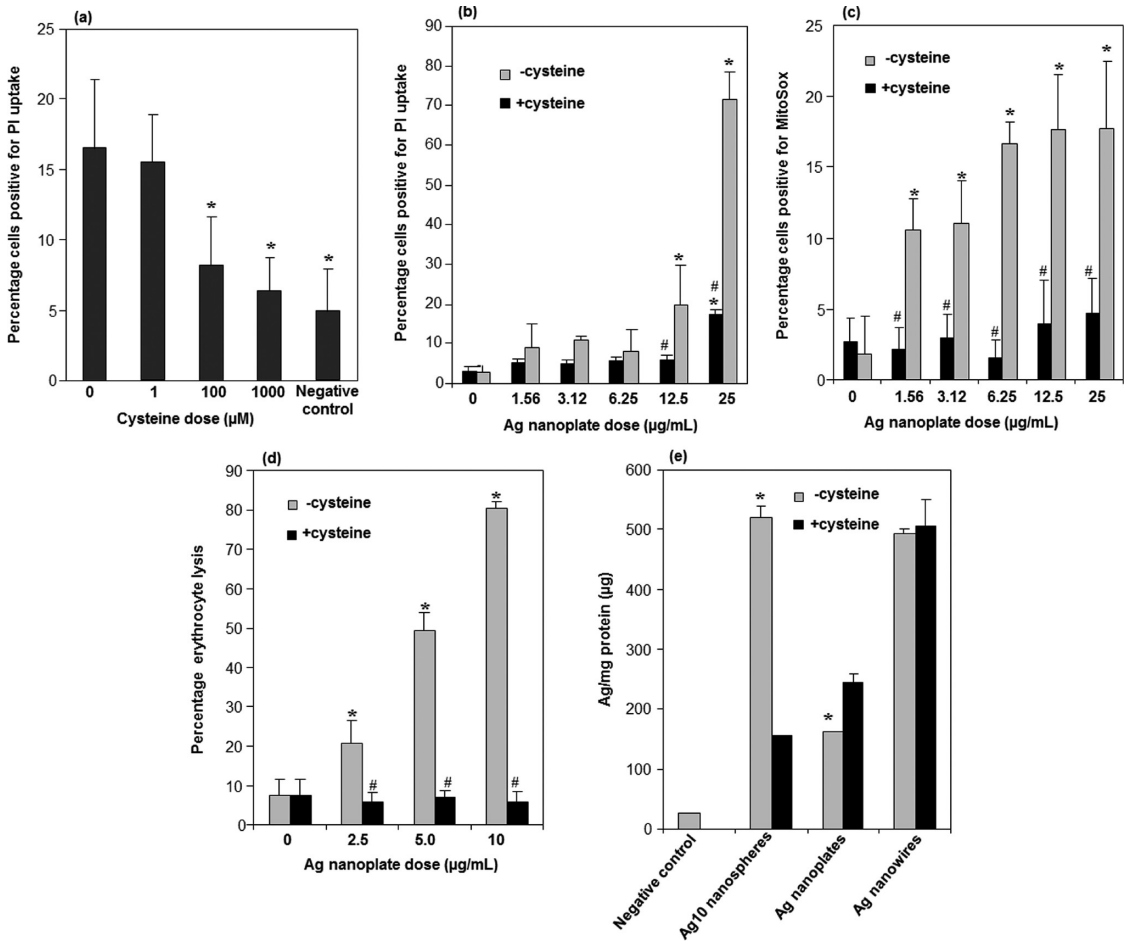

Figure 6. Surface passivation of Ag nanoplates by cysteine eliminated their cytotoxic effects. Ag-nanoplate suspensions in water were replenished with 1 mM cysteine-HCl and stirred overnight. The particles were washed in water and resuspended in L-15 medium containing alginic acid. (a) Effect of coating with incremental concentrations of cysteine on the induction of cytotoxicity by 10 μg/mL of Ag-nanoplate suspension. (b) Comparative effects of cysteine coating on the cytotoxic effects of incremental doses of Ag nanoplates. (c) Comparative effects of cysteine coating on mitochondrial superoxide generation by incremental doses of the Ag nanoplates. (d) Comparative effect of cysteine coating on the induction of RBC lysis by incremental doses of the Ag nanoplates. (e) ICP-MS analysis to quantify the Ag content of cells treated with cysteine-coated and original Ag10 nanospheres, Ag nanoplates, and Ag nanowires. While cysteine coating reduced the total Ag content in cells treated with the nanospheres, similar coating effects were not seen in the Ag-nanoplate- or Ag-nanowire-treated groups. Experiments were repeated three times, using triplicates in each group. * Statistically significant difference from control ($p < 0.05$). # statistically significant difference from untreated ($p \leq 0.001$). Error bars represent standard deviation from average value.

and surface passivation has been shown to reduce the electro-catalytic property.[27] In order to assess the contribution of surface reactivity to the toxicity of Ag nanoplates more directly, we asked whether surface coating with cysteine could reduce this material's toxicity. Utilizing the cytotoxicity that is induced by 10 μg/mL Ag nanoplates, we demonstrated that increasing the cysteine concentration from 10 to 1000 μM leads to a progressive reduction and even elimination of PI uptake (Figure 6a). This observation also held true with incremental doses of the Ag nanoplates (Figure 6b). The same protective effects could also be seen in studying superoxide generation by incremental doses of the Ag nanoplates (Figure 6c). Cysteine passivation likewise reversed the membranolytic activity of Ag nanoplates in RBC (Figure 6d).

To test more directly if the decreased toxicity of cysteine-coated nanoplates is due to the suppression of surface reactivity as compared to a change of bioavailability, ICP-MS was performed with cysteine-coated as well as original Ag nanoplates as shown in Figure 3. Thus, while the cysteine coating of Ag10 nanospheres reduced the total cellular Ag content at least 4-fold, passivation of nanoplate and nanowire surfaces did not elicit similar effects (Figure 6e). In fact, coating of the nanoplate surfaces was accompanied by a slight increase in cellular Ag content (Figure 6e). This observation suggests different mechanisms of toxicity of Ag nanoplates versus Ag nanospheres, and is consistent with the reactivity of the Ag nanoplate surfaces, which leads to cell membrane damage.

Ag Nanoplates Elicited Higher Toxicity in Zebrafish Embryos than Other Ag Nanoparticles and the Toxicity Could Be Eliminated or Diminished by Passivation of the Nanoplate Surface. To compare the cellular results to *in vivo* outcome, we used the zebrafish embryo (*Danio rerio*) as an organism

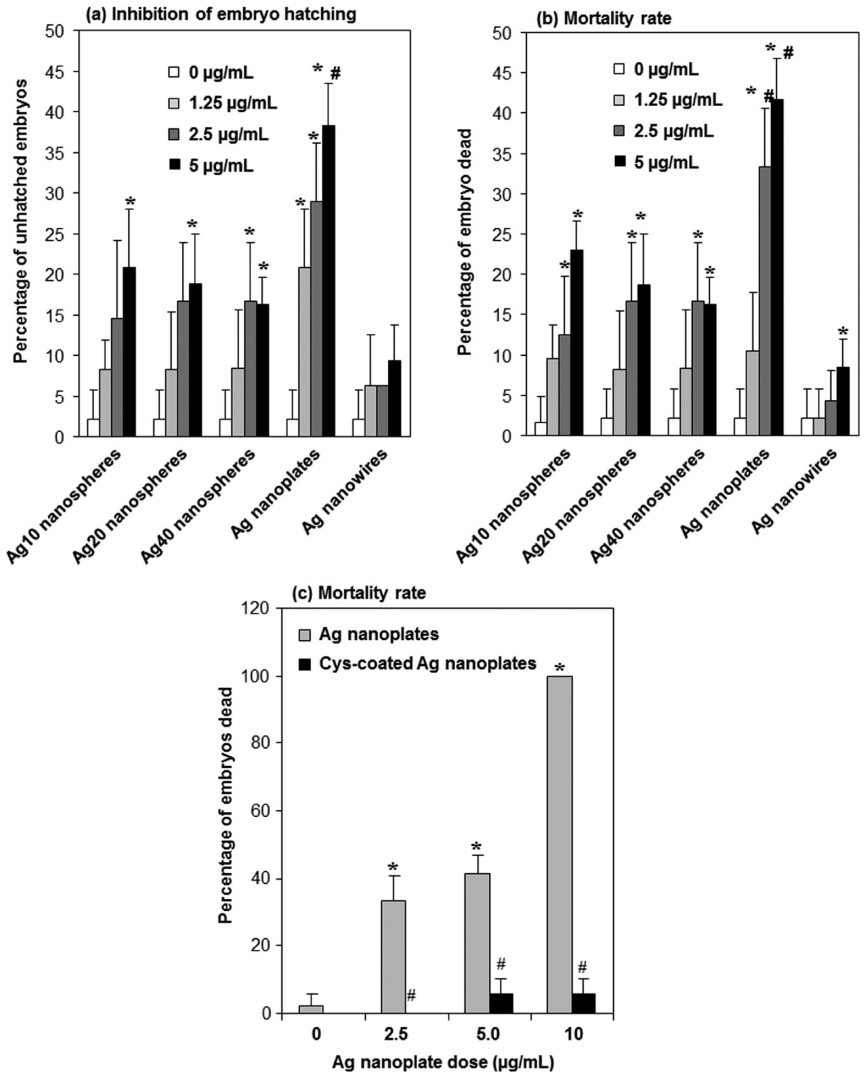

Figure 7. Zebrafish embryo toxicity induced by Ag nanoparticles. Zebrafish embryos exposed to increasing doses of Ag nanoparticles in Holtfreter's medium were assessed for: (a) inhibition of embryo hatching at 48 hpf; (b) mortality rate at 120 hpf; and (c) passivating Ag nanoplates with cysteine abolished the zebrafish embryo toxicity. Ag nanoplates reacted with cysteine HCl (as detailed in Figure 6) were used to treat zebrafish embryos and the mortality rates were compared to uncoated nanoplates. The average value was calculated for a total of 36 embryos in three experiments, using 12 embryos per group. Experiments were repeated three times with triplicate samples in each group. * Statistically significant difference from control ($p < 0.05$). # statistically significant difference from untreated Ag nanoplates ($p \leq 0.001$). Error bars represent the standard deviations from the average values.

that is increasingly being recognized for its use as a model for studying chemical and nanomaterial toxicity.[28−31] To avoid the agglomeration of the Ag nanoparticles in Holtfreter's medium, 100 ppm alginate was used to stabilize the particles. Table 1 shows the average hydrodynamic diameters of Ag nanoparticles suspended in Holtfreter's medium supplemented with alginic acid. Ag nanoplates showed the best dispersion. Zebrafish embryos were exposed to the Ag-nanoparticle suspensions, starting at 4 h postfertilization (hpf) and analyzed every 24 h for up to 120 hpf. Toxicity was scored as percentage of embryos failing to hatch or dying. While most of the nanoparticles induced a dose-dependent increase in hatching failure or embryonic mortality, Ag nanoplates were clearly the most toxic, leading to 100% mortality rate at a dose of 10 μg/mL (Figure 7a,b). There were no significant differences among spherical nanoparticles, while Ag nanowires elicited the least impact. Ag nanoplates also induced more morphological defects than other nanoparticles as outlined in Figure S5 (Supporting Information). We also used cysteine-coated Ag nanoplates to determine if surface passivation ameliorates embryo toxicity. Indeed, cysteine coating prevented embryonic mortality at a lower Ag nanoplate dose while also significantly suppressing lethality at higher Ag nanoplate concentrations (Figure 7c).

ICP-MS Analysis and Rhodamine Isothiocyanate Labeling of the Nanoparticles to Determine Ag Bioavailability. We used ICP-MS to determine the kinetics of Ag release in

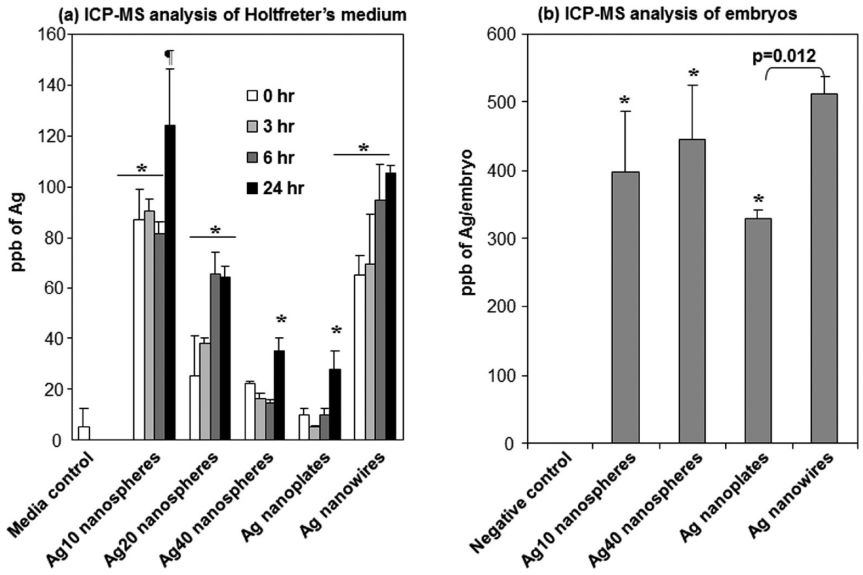

Figure 8. ICP-MS analysis of zebrafish embryos treated with Ag nanoparticles. (a) ICP-MS analysis of Ag release into the Holtfreter's medium. Ag-nanoparticle suspensions (5 μg/mL) were prepared in Holtfreter's medium containing alginic acid and assayed for Ag release at incremental time intervals as detailed in Figure 3b. (b) Ten zebrafish embryos, treated with 5 μg/mL Ag nanoparticles for 48 h were washed and homogenized using a probe sonicator. The total Ag content of the homogenates was determined after acid hydrolysis. ICP-MS results showed comparable amount of total Ag in embryos treated with Ag nanosphere and Ag nanowire but was slightly lower in Ag-nanoplate-treated embryos. The average amount of Ag calculated from three replicates (10 embryos in each) is expressed as ppb of Ag per individual embryo. Experiments were repeated three times with triplicate samples in each group. * Statistically significant difference from media control/untreated zebrafish embryos ($p \leq 0.05$). ¶ statistically significant differences from media control/untreated zebrafish embryos and other types of Ag nanoparticles ($p \leq 0.05$).

Holtfreter's medium as well as to measure total Ag content in exposed zebrafish embryos (Figure 8). While all the Ag nanoparticles showed time-dependent Ag shedding in Holtfreter's, Ag10 nanospheres generated the highest level of Ag ions in incubation medium and Ag nanoplates showed the lowest release (Figure 8a). This demonstrates that, like the cellular studies, the higher toxicity of the Ag nanoplates cannot be ascribed to particle dissolution and shedding of Ag ions. This conclusion was further strengthened by measurement of the total Ag content in the zebrafish embryos, which demonstrated that while the embryonic metal content following incubation with Ag nanospheres and Ag nanowires achieved levels of 400−500 ppb, the measured metal contents following exposures were significantly lower at 328 ppb (Figure 8b).

To visualize the site of nanoparticle association with zebrafish embryo, we attempted to label Ag nanoplates, nanospheres, and nanowires with rhodamine isothiocyanate (RITC), a fluorescent dye. The fluorescence spectra of RITC-labeled particles were analyzed at 640 nm in order to assess the efficiency of labeling. These measurements demonstrated that while Ag nanoplates could be labeled effectively, the labeling efficiencies of Ag nanospheres and Ag nanowires were low (Figure S6a, Supporting Information). We used a transgenic zebrafish strain expressing green fluorescence protein (GFP) in vascular endothelial cells under the control of the flk-1 gene that encodes the vascular endothelial growth factor receptor 2. This leads to the development of green fluorescent blood vessels as a result of the expression of Flk-GFP in the developing zebrafish embryos. The use of the RITC-labeled Ag nanoplates to perform confocal microscopy in these transgenic embryos, demonstrated that the RITC-labeled nanoplates are capable of binding to the chorion (the membrane surrounding the embryo), but did not show any particle uptake in embryonic tissues (Figure S6b). Interestingly, the RITC-labeled nanoplates did not interfere with embryo hatching nor damage the Flk-1 expression in the vasculature of the larvae, while unlabeled nanoplates were toxic to the embryos and disrupted vascular development (Figure S6b). A likely explanation for the reduced toxicological effects of RITC labeling is that it contains thiol groups similar to cysteine that could contribute to passivating the plate surfaces (Figure S7b-c, Supporting Information).

DISCUSSION

In this paper, we demonstrate that crystal defects in plate-shaped Ag nanoparticles exhibit toxicological effects that differ from those of Ag nanospheres and Ag nanowires. These differences apply to both *in vitro* assessment of cytotoxicity and superoxide generation in a fish gill cell line, as well as the *in vivo* assessment of zebrafish development and mortality. Cellular assays showed that Ag nanoplates could induce toxic oxidative stress that was not directly related to Ag shedding or bioavailability. Coupled with a lack of evidence of cellular uptake of the nanoplates, we hypothesized

that the surface membrane damage in the cells results from particle-mediated surface reactivity. This notion was strengthened by the finding that the membranolytic effects as well as cellular toxicity were eliminated when Ag nanoplates were physically segregated from the cells. Analysis using HRTEM demonstrated the prevalence of crystal defects in the majority of Ag nanoplate surfaces while cysteine coating of the nanoplates diminished their toxicity. Similar observations were made when comparing the toxicity of Ag nanoplates with Ag nanospheres and nanowires in the zebrafish embryo, with the nanoplates inducing a high rate of hatching interference and lethality that could be eliminated by cysteine coating. Taken together, this study demonstrates the contribution of crystal defects in inducing oxidative stress injury by Ag nanoplates during direct physical contact with the target system. Execution of the study in a fish cell line also reflected higher levels of toxicity of the Ag nanoplates in zebrafish embryos, establishing a predictive toxicological paradigm that enables *in vitro* observations to be compared to *in vivo* biological outcomes.

The potential ecological impact of Ag nanoparticles has been highlighted by several studies in bacteria, invertebrates, and vertebrates, including fish models.[3,32] The majority of these studies ascribed the toxicity of Ag nanoparticles to the release of Ag ions from their surfaces.[10,29] Although several reports highlight the influence of exposure conditions and particle size in determining the release of Ag ions from nanomaterials,[10] there has been no experimental evidence showing the direct contribution of crystal defects in mediating Ag-nanoparticle toxicity. This could be due to the fact that most studies to date have focused on spherical Ag nanoparticles that are relatively free of crystal defects. However, recent reports have outlined the importance of stacking faults in contributing to the higher electrocatalytic activity of Ag nanoplates and Ag nanodiscs.[33] In fact, the superior electrocatalytic properties of Ag nanoplates make them the preferred form for industrial catalysis. It is now also recognized that Ag nanoplates have higher antibacterial activity than other forms of Ag nanoparticles.[1] Thus, the increased interest in plate-shaped Ag nanoparticles for industrial as well as consumer product applications should consider the biological hazard potential of these novel use applications.

Examination of the Ag nanoplates by HRTEM demonstrated that alternating {111} and {200} stacking planes create material defects (Figure 5a–c) that are enriched for dangling bonds, which could confer higher electrocatalytic activity due to the local increase in electron density. These defects could lead to the disruption of biomolecules or cellular structures that make physical contact with the defect sites or the free oxygen radicals generated at these sites.[34] The injury could result in membrane disruption and generation of cellular oxidative stress, as demonstrated by assaying for calcein release, RBC lysis, and superoxide production. Moreover, NAC, a potent antioxidant, significantly suppressed the cytotoxicity and superoxide production in RT-W1 cells (Figure 2b,d). While Ag ions could induce oxidative stress through glutathione depletion,[35] ICP-MS analysis demonstrated a lower dissolution rate and cellular content of Ag in cells treated with Ag nanoplates in spite of their dramatic increase in rates of toxicity. This suggests that the enhanced toxicity potential of the nanoplates is not only due to Ag ion shedding. Further evidence that Ag shedding is not the principal mechanism of Ag nanoplates toxicity is the reduction in toxicity when the Ag nanoplates are physically prevented from binding to RT-W1 cells through partitioning. Although soluble Ag can induce erythrocyte lysis (Figure S3, Supporting Information), disruption of the RBC surface membrane is a signature property of particles with high surface reactivity.[25] The same holds true for Ag nanoplates, which induce membranolysis upon direct contact with RBC but not when the nanoplates were sequestered in a dialysis bag. The notion of surface reactivity is strengthened by demonstrating that passivation of the surface of Ag nanoplates by cysteine coating could eliminate their cytotoxicity and membranolytic potential (Figure 6a–d). In addition to the increased surface reactivity, the lowering of the binding energy by planar surface of the Ag-nanoplates could play a role in promoting the toxicological interactions at the nanobio interface. This includes a possible role for the dangling bonds at the crystal defect sites, which could contribute to promoting the binding to the cell membrane and free radical generation, both of which may contribute to cytotoxicity. While it would have been satisfying to obtain quantitative structure–activity analysis that relates the number of defects to biological outcome, this will require the development of a carefully constructed Ag-nanoplate library that systematically varies the percentage of the surface area covered by crystal defects. While we have been able to achieve the synthesis of combinatorial ENM libraries to study the toxicity of cationic nanoparticles,[36] silica nanoparticles,[37] ZnO nanoparticles,[22] and multiwalled carbon nanotubes,[38] the synthesis of a combinatorial Ag nanoplate library falls outside of the scope of the current study. Nonetheless, the comparative analysis of crystal defects on different Ag nanoparticle shapes and the ability to activate the Ag nanoplate surface suffice to demonstrate the involvement of crystal defects in cellular as well as embryo toxicity. This result is important from the perspective of metallic surface defects in the catalysis of biological injury.

We used zebrafish embryos to validate the cellular observations of a higher rate of Ag-nanoplate toxicity. The zebrafish is now recognized as an appropriate animal model for toxicological assessment of ENMs.[9,13,16,29]

This includes the use of this organism for studying shape-dependent toxicity of nickel nanoparticles, in which it was demonstrated that dendrimer-shaped nanoparticles show a higher level of toxicity than spherical particles premised on the principle of delayed clearance from the gut of zebrafish larvae.[13] In agreement with our cellular observations, the mortality rate in zebrafish embryos was the highest for Ag nanoplates in spite of a general dose-dependent toxicological effect of all the Ag nanoparticles. Other sublethal effects, such as inhibition of embryo hatching and morphological defects, were also prominent with Ag nanoplates. ICP-MS showed that shedding of Ag ions into Holtfreter's medium as well as bioavailability of Ag were relatively low in Ag nanoplate-treated embryos. These results suggest that the induction of embryo mortality and the sublethal effects of the Ag nanoplates are mediated by a mechanism other than Ag shedding or bioavailability. Thus, while increased organ retention of dendrimer-shaped Ni nanoparticles may explain the higher level of toxicity in the gut of zebrafish larvae, neither the total level of Ag bioavailability or tissue retention could explain the increased toxicity of Ag nanoplates. However, it remains to be determined at the anatomical level how the surface reactivity of Ag nanoplates leads to lethality and the induction of morphological abnormalities in the embryo prior to functioning of the gut. The involvement of surface reactivity was confirmed by the reduced embryo mortality and hatching interference when the nanoplates were coated with cysteine (Figure 7c). While RITC labeling demonstrated that the Ag nanoplates bind to the chorion, we were not able to observe particle uptake in the tissues or organ-specific retention in the embryo (Figure S6b, Supporting Information). Whether interactions with the chorion are sufficient to explain nanoplate toxicity is unknown and warrants further study of the pathogenesis of injury at the intact organism level, including the use of newly emerging technology to perform histopathological analysis that can be related to ENM injury responses as demonstrated for Ni nanoparticles.[13] Since Ag nanospheres have been demonstrated to be taken up into zebrafish embryos,[29] one possibility is that nanoplate labeling is not efficacious to yield the resolution necessary for detecting Ag nanoplates in the embryonic tissues. In addition, RITC labeling leads to passivation of the Ag nanoplate surface, which could also interfere with bioavailability.

Toxicity testing in fish has been recognized as a "gold standard" for ecotoxicology. However, the high maintenance cost, ethical considerations, and reduced ability to obtain mechanistic information, makes cellular models an attractive alternative or precursor to the performance of fish studies. This is exemplified by the findings here, in which we demonstrate the use of a primary fish gill cell line to conduct mechanistic studies implicating the role of surface defects in Ag nanoplate toxicity, which was subsequently applied to the study of zebrafish embryos. The utility of *in vitro* cellular assays for assessing pathway-based material toxicity enables the establishment of property-activity analysis that can be used to speed up ENM assessment, including the prioritization of more labor-intensive *in vivo* studies. The fish gill cell line is also valuable for performing comparative analysis with mammalian cells, including demonstrating species-specific differences in the sensitivity to Ag nanoparticles. In this regard, our provisional observations suggest that RT-W1 cells are more sensitive to the effects of nano-Ag compared to mammalian cell lines on a per weight basis and that the cells can be useful for exploring species-specific differences.

CONCLUSIONS AND PROSPECTS

We report that surface reactivity as a result of crystal defects increases the toxicity of Ag nanoplates vs other Ag nanoparticles. We tested a small library of Ag nanoparticles that included nanospheres of varying size (10, 20, and 40 nm diameter), nanoplates (32 nm) and nanowires (65 nm x 20 μm) for their differential toxicity in RT-W1 cells and zebrafish embryos. Ag shedding by Ag nanoplates and Ag bioavailability were considerably lower than other Ag nanoparticles. The enhanced propensity of Ag nanoplates to induce plasma membrane damage was demonstrated by calcein release in RT-W1 and membrane lysis in RBC. Moreover, physical contact was required for this membranolytic activity. Analysis by HRTEM showed a high prevalence of crystal defects in Ag nanoplates compared to spherical Ag nanoparticles. In an effort to suppress the surface reactivity, surface coating with cysteine was used to reduce Ag nanoplate toxicity. Taken together, we show that the increased surface reactivity of Ag nanoplates is due to the expression of crystal defects that should be considered as another important mechanism for Ag nanoparticle toxicity, in addition to Ag ion shedding.

MATERIALS AND METHODS

Nanomaterials Sources and Preparation for Biological Experimentation. A panel of PVP-coated Ag nanoparticles with different shapes and sizes were obtained from Nanocomposix (4878 Ronson Court, San Diego, CA). The stock particle suspensions were further diluted in water (25 μg/mL) and used for size determination by dynamic light scattering (DLS), XRD, and TEM.

Transmission Electron Microscope Imaging of Ag Nanoparticles. A drop of each particle sample in deionized water was applied to a TEM grid and evaporated at room temperature. The particle

images were taken with a JEOL 1200 EX TEM microscope. High-resolution transmission electron microscopy images were obtained with a FEI Titan 80/300 microscope equipped with a Cs corrector for the objective lens, high angle annular dark-field detector (HAADF), GATAN postcolumn imaging filter, and a cold field-emission gun operated at an accelerating voltage of 300 kV.

X-Ray Diffraction Measurements. A drop of each particle sample in deionized water was applied in the sample holder and evaporated at room temperature. The Ag nanoparticles were loaded into a PANalytical X'Pert MPD PRO diffracting system, equipped with Ni-filtered CuK_α (λ = 0.154 nm) radiation, 1/4° fixed divergence, primary and secondary Soller slit with a 0.04 rad aperture, circular sample holder with 16 mm diameter, and X'Celerator detector. A continuous scan was performed to cover 20−80° 2θ. The structural and microstructural parameters were extracted through Rietveld refinement using the Brass program. Background, scale factor, unit cell parameters, and Gaussian as well as Lorentzian half-widths were simultaneously refined, followed by crystalline microstrain analysis.

Surface Coating of Ag Nanoplates with Cysteine HCl. Ag nanoplates, suspended in deionized water, were surface coated with cysteine-HCl. Working solutions of the Ag nanoplates suspended at 10 μg/mL were replenished with incremental amounts of cysteine-HCl to yield final concentrations of 1, 100, and 1000 μM. These solutions were stirred overnight (16 h) at room temperature, following which the Ag nanoplates were separated by ultracentrifugation at 20000× *g* for 60 min. These particles were washed three times using deionized water and resuspended in Liebovitz's L-15 cell culture or Holtfreter's medium by sonicating 15 s with a probe-sonicator (VibraCell, Sonics, CT) at 30 W, for evaluating the cytotoxicity and zebrafish embryo toxicity, respectively.

Preparation of Ag Nanoparticles in Exposure Media. Freshly prepared working concentrations of the Ag nanoparticles for the cellular studies were prepared in L-15 medium to provide a mass-dose concentration range of 0−25 μg/mL. While L-15 medium is supplemented with 10% fetal bovine serum (FBS) to grow and initially to establish RT-W1 cells in 384 well plates, the FBS was omitted during the performance of the MitoSox Red and PI uptake assays because of the interference of serum proteins with the toxicological assessment. To stabilize the particle suspensions during this phase of the work, alginic acid (Sigma Aldrich, St. Louis, MO) was used as an environmentally relevant and biocompatible dispersant during zebrafish embryo exposures.[9] Alginic acid was introduced to the particle working solutions at a final of 100 ppm, following which the suspensions were sonicated for 15 s with a probe sonicator. The alginate-supplemented particle suspensions were also used for the physicochemical characterization (agglomeration size, and zeta potential) as described in Tables 1 and 2. During the calculation and interpretation of the cellular response data, the particle mass-dose concentrations were recalculated to surface area dose as described below. Mass-dose concentrations of 0−25 μg/mL correspond to surface area doses of 0−35 × 10^{-4} m^2, depending upon the shape of the Ag nanoparticles.

For zebrafish experiments, we used Holtfreter's medium, which contains 3.5 g NaCl, 0.20 g $NaHCO_3$, 0.05 g KCl, and 0.12 g $CaCl_2$ dihydrate in 1000 mL of deionized water, at pH 6.5−7. The filtered solution was supplemented with alginic acid at a concentration of 100 ppm. Aliquoted Ag nanoparticle stock solutions were added to the Holtfreter's medium supplemented with alginate and sonicated for 15 s using a probe sonicator.

Inductively Coupled Plasma-Mass Spectrometry. Inductively coupled plasma-mass spectrometric analysis was performed to detect Ag metal release from nanoparticles suspended in exposure media (L-15 and Holtfreter's media); 10 μg/mL of each of the Ag nanoparticles were suspended in 1 mL of the respective media for 0, 3, 6, and 24 h before undissolved particles were spun down at 100000× *g* for 4 h and the supernatants collected. Fifty μL of supernatant solution was added to a Teflon container and acidified with 5 mL of pure nitric acid and digested on a hot plate for 6 h. The nitric acid was evaporated and replenished with 3 mL 5% nitric acid. Ag metal concentrations were measured in the 5% nitric acid solution by a Perkin-Elmer SCIEX Elan DRCII mass spectrometer. The average values were calculated from three replicates for each group.

ICP-MS was also used to assess the total Ag content in RT-W1 cells exposed to Ag nanoparticles. The initial cultures were started in 6 well plates in the presence of L-15 medium +10% FBS to get 80% confluency. The culture medium was replaced with a suspension of 5 μg/mL Ag nanoparticles made up in L-15 medium supplemented alginic acid, and incubated at room temperature for 24 h. The culture medium was removed and cells were rinsed three times in PBS. Following the addition of 500 μL of PBS, the cells were scraped off with a scraper, transferred to an Eppendorf tube and sonicated for 30 s with the probe-sonicator at 30 W to homogenize the cells. The probe was washed with 500 μL PBS that was added to the homogenate. Fifty microliters of each homogenate was transferred to a Teflon container and acidified with 5 mL of pure nitric acid. The rest of the procedure is as described above. The concentration in each sample was expressed as ppb of Ag/mg of cellular protein.

For Ag quantification in zebrafish embryos, 10 zebrafish embryos were treated with 100 μL of a 5 μg/mL concentration for each Ag nanoparticle in Holtfreter's medium. After 48 h of treatment, the embryos were washed thrice in PBS. The washed embryo pellets were resuspended in 500 μL water and sonicated for 30 s with a probe sonicator at 30 W. Each homogenate received an additional 500 μL of water from which 50 μL was used to perform ICP-MS analysis, as detailed above. The average value from three replicates was used to express the Ag content per embryo in ppb Ag.

Cell Culture and Coincubation with Ag Nanoparticles. The RT-W1 fish cell line was originally derived from the gill tissue of the rainbow trout, *Oncorhynchus mykiss*. RT-W1 is a primary fish cell line that is frequently used to evaluate chemical toxicity.[39] A starting culture was obtained from American Type Culture Collection (Manassas, VA) (ATCC #CRL-2523) and grown in a CO_2-free environment in L-15 medium supplemented with 10% FBS, 2 mM L-glutamine, 100 IU/mL penicillin and 100 μg/mL streptomycin. These cells were maintained in 25 cm^2 culture flasks, in which the cells were passaged once every three days at 70−80% confluency. For the purposes of conducting high-throughput toxicity screening, 5000 cells were transferred into each well of a 384 well tissue culture plate (Greiner bio-one, NC), followed by overnight culture at room temperature (24 °C). At this point, the FBS-supplemented L-15 medium was removed and the wells washed twice with PBS before receiving 50 μL of the various Ag nanoparticle suspensions prepared in L-15 supplemented with 100 ppm alginic acid. Prior experimentation confirmed that the alginic acid is biocompatible and that the slow-growing cells could be maintained in serum-free conditions for at least 24 h without a decline in cell viability. Moreover, there was no decline or exaggeration in the oxidative stress response of the cells during comparative analysis at 6, 12, and 24 h. The nanoparticle exposures were carried at seven different particle concentrations that were expressed in both mass and surface area metrics. Control wells received exposure medium without nanoparticles.

The high-throughput screening assays involve the use of epifluorescence microscopy to assess cellular superoxide generation as well as decrease in cell viability. This was accomplished by introducing 25 μL of one of two dye cocktails that either included MitoSox Red (5 μM) plus Hoechst 33342 (1 μM), or propidium iodide (PI) (5 μM) plus Hoechst 33342 (1 μM) into each well by automated robotic equipment. MitoSox Red assesses mitochondrial superoxide generation, while PI nuclear uptake reflects increased membrane permeability in dying cells. Cellular fluorescence images were acquired using an automated Image-Xpress^{micro} (Molecular Devices, Sunnyvale, CA) epifluorescence microscope. The images were analyzed by MetaXpress software (Molecular Devices, Sunnyvale, CA) to score the percent positive responses for each assessment parameter. Hoechst 33342 dye was used to count the total cell number of cell nuclei using the following blue channel settings: minimum width = 3 μm (~3 pixels), maximum width = 10 μm (~7 pixels), threshold intensity above background = 100 gray levels. The corresponding red channel settings for PI and

MitoSox Red were: minimum width = 5 μm (~6 pixels), maximum width = 30 μm (~22 pixels), threshold intensity above background = 500 gray levels. Thus, the cells showing increased fluorescence above the threshold were scored as percent MitoSox Red or PI-positive cells by using the total number of Hoechst 33342 stained nuclei. Each experiment was repeated three times with six replicates in each group. The statistical significance was calculated using a paired *t* test.

Approach for Converting Particle Mass Dose into Surface Area Dose Metrics. Since surface area dose is an appropriate metric for quantitative assessment of the property-activity relationships of high surface reactive ENMs,[40,41] we also included surface area dose calculations to compare different Ag nanoparticles. The surface areas of nanospheres, nanoplates, and nanowires were calculated based on the mathematical formulas for spheres, discs, and cylinders. The individual surface areas were then multiplied with the total number of nanoparticles present in 1 mg of material to get the specific surface area of each type of nanoparticle. The total number of nanoparticles present in 1 mg sample was provided by the supplier (see Table 1). With knowledge of the specific surface area for each type of Ag nanoparticle in 1 mg of material, the surface area for 0, 1.56, 3.12, 6.25, 12.5, and 25 μg material could be calculated.

Fluorescence Microscopy to Determine Cell Membrane Damage during Direct and Indirect Exposure to Ag Nanoplates. RT-W1 cells were grown in 24 well plates (Becton Dickinson Labware, NJ). Each well received 10^6 cells suspended in 1 mL growth medium. Cells were initially grown overnight in L-15 medium containing 10% FBS, followed by washing in PBS and then replenished with fresh L-15 medium supplemented with 100 ppm of alginic acid, as described above. Triplicate wells received the direct addition of 10 μg/mL Ag nanoplates to the growth media, while an additional three wells received 500 μL of growth medium plus the addition of a similar amount of Ag nanoplates included in 500 μL medium in a sealed dialysis tube (Slide-A-Lyzer Mini dialysis units, Thermo Scientific, Waltham, MA) that has a 3.5 KD cutoff pore size. The dialysis container was mounted such that it was totally immersed in the cell culture medium. The tissue culture plate was placed on a shaker (Thermo Scientific) at room temperature for 24 h. The supernatants were removed and a mixture of Hoechst 33342 (1 μM), Calcein-AM (5 μM) and PI (5 μM) added to the cells in PBS for another 30 min. The cells were removed and viewed under a fluorescence microscope (Observer D1. Carl Zeiss, Germany). The fluorescence images were analyzed using Image J software (NIH, Bethesda, MD) and the average fluorescence intensity of at least 30 randomly selected cells was used to express quantitatively the loss of green fluorescence intensity (calcein) or the increase in nuclear PI uptake for each treatment group.

Use of Erythrocyte Lysis to Quantify the Membranolytic Potential of Ag Nanoparticles. Heparinized mouse blood was collected from Balb/C mice and the RBC rinsed in PBS. The RBC were suspended at 1×10^9 cells per mL and directly exposed to increasing concentrations of Ag nanoparticles for 4 h at 37 °C. PBS-exposed or 0.025% Triton X-100 treated cells served as negative and positive controls, respectively. The samples were centrifuged and the hemoglobin absorbance in the supernatants was measured at 540 nm in a microplate reader (M5e, Molecular Devices, USA). The values were normalized according to the positive control, which represents 100% cell lysis. The average value from 9 independent observations was plotted in a graph. To compare the direct lysis to the possible effects of Ag shedding, Ag nanoparticles were also introduced in dialysis tubing for 4 h and lysis calculated as detailed above.

Zebrafish Embryo Exposure to Ag Nanoparticles. Working Ag nanoparticle solutions were prepared in Holtfreter's medium at final concentrations of 0, 1.25, 2.5, and 5 μg/mL, as detailed above. Zebrafish embryos were collected in Holtfreter's medium 2 hpf from mating cages. Embryos were visually assessed for viability and the healthy specimens transferred into 96-well plates, including 1 embryo per well. Beginning at 4 hpf, the spherical stage of the embryo was exposed to 100 μL/well of Ag nanoparticles in Holtfreter's medium or a control solution without nanoparticles. Three replicate trials that involved 12 embryos per treatment group were performed. The rate of embryo hatching, survival, and morphological defects were assessed at 24, 48, 72, 96, and 120 hpf. Hatching rate was expressed as the number of embryos that were completely hatched by 72 hpf, while the mortality rate was expressed as the total number of dead embryos at 120 hpf.

Conflict of Interest: The authors declare no competing financial interest.

Acknowledgment. This work is supported by the National Science Foundation and the Environmental Protection Agency under Cooperative Agreement Number DBI 0830117. Any opinions, findings, conclusions, or recommendations expressed herein are those of the author(s) and do not necessarily reflect the views of the National Science Foundation or the Environmental Protection Agency. This work has not been subjected to an EPA peer and policy review. Key support was provided by the US Public Health Service Grants U19 ES019528 (UCLA Center for NanoBiology and Predictive Toxicology), RO1 ES016746, and RC2 ES018766. S.G. acknowledges the suggestions from and help of Dr. Kristin Schirmer (Eawag, Switzerland) in designing the fish cell line studies.

Supporting Information Available: UV−visible absorbance spectra of Ag nanoparticles of various shapes, transmission electron microscopy to show RT-W1 stress responses but limited Ag nanoparticle uptake except for Ag nanowires, demonstration of the mass-dose response to Ag nanoparticles in the erythrocyte membrane lysis assay, HRTEM of Ag-nanoplates showing the prevalence of crystal defects, differential effects of Ag nanoparticles toward inducing morphological abnormalities in hatched and surviving zebrafish embryos, fluorescence labeling of Ag nanoparticles with Rhodamine B isothiocyanate and confocal microscopy of zebrafish embryo treated with labeled Ag nanoplates, confocal microscopy to demonstrate binding of RITC-coated Ag nanoplates to the chorion of transgenic zebrafish embryos but not to hatched larvae, Rhodamine B isothiocyanate coating reduces the embryonic toxicity of the Ag nanoplates. This material is available free of charge *via* the Internet at http://pubs.acs.org.

REFERENCES AND NOTES

1. Morones, J. R.; Elechiguerra, J. L.; Camacho, A.; Holt, K.; Kouri, J. B.; Ramírez, T. J.; Yacaman, M. J. The Bactericidal Effect of Silver Nanoparticles. *Nanotechnology* **2005**, *16*, 2346.
2. Navarro, E.; Piccapietra, F.; Wagner, B.; Marconi, F.; Kaegi, R.; Odzak, N.; Sigg, L.; Behra, R. Toxicity of Silver Nanoparticles to *Chlamydomonas reinhardtii*. *Environ. Sci. Technol.* **2008**, *42*, 8959–8964.
3. Wijnhoven, S. W. P.; Peijnenburg, W. J. G. M.; Herberts, C. A.; Hagens, W. I.; Oomen, A. G.; Heugens, E. H. W.; Roszek, B.; Bisschops, J.; Gosens, I.; Van De Meent, D.; et al. Nano-Silver: A Review of Available Data and Knowledge Gaps in Human and Environmental Risk Assessment. *Nanotoxicology* **2009**, *3*, 109–138.
4. Glover, R. D.; Miller, J. M.; Hutchison, J. E. Nanoparticle Dynamics on Surfaces and Potential Sources of Nanoparticles in the Environment. *ACS Nano* **2011**, *22*, 8950–8957.
5. Zhao, C.-M.; Wang, W.-X. Comparison of Acute and Chronic Toxicity of Silver Nanoparticles and Silver Nitrate to *Daphnia Magna*. *Environ. Toxicol. Chem.* **2011**, *30*, 885–892.
6. Griffitt, R. J.; Luo, J.; Gao, J.; Bonzongo, J.-C.; Barber, D. S. Effects of Particle Composition and Species on Toxicity of Metallic Nanomaterials in Aquatic Organisms. *Environ. Toxicol. Chem.* **2008**, *27*, 1972–1978.
7. Davies, P. H.; Goettl, J. P., Jr; Sinley, J. R. Toxicity of Silver to Rainbow Trout (*Salmo gairdneri*). *Water Res.* **1978**, *12*, 113–117.
8. Ji, J. H.; Jung, J. H.; Kim, S. S.; Yoon, J. U.; Park, J. D.; Choi, B. S.; Chung, Y. H.; Kwon, I. H.; Jeong, J.; Han, B. S.; et al. Twenty-Eight-Day Inhalation Toxicity Study of Silver Nanoparticles in Sprague-Dawley Rats. *Inhal. Toxicol.* **2007**, *19*, 857–871.
9. George, S.; Xia, T.; Rallo, R.; Zhao, Y.; Ji, Z.; Lin, S.; Wang, X.; Zhang, H.; France, B.; Schoenfeld, D.; et al. Use of a High-Throughput Screening Approach Coupled with *In Vivo*

Zebrafish Embryo Screening to Develop Hazard Ranking for Engineered Nanomaterials. *ACS Nano* **2011**, *5*, 1805–1817.
10. Liu, J.; Sonshine, D. A.; Shervani, S.; Hurt, R. H. Controlled Release of Biologically Active Silver from Nanosilver Surfaces. *ACS Nano* **2010**, *4*, 6903–6913.
11. Brown, S. C.; Kamal, M.; Nasreen, N.; Baumuratov, A.; Sharma, P.; Antony, V. B.; Moudgil, B. M. Influence of Shape, Adhesion and Simulated Lung Mechanics on Amorphous Silica Nanoparticle Toxicity. *Adv. Powder Technol.* **2007**, *18*, 69–79.
12. Pal, S.; Tak, Y. K.; Song, J. M. Does the Antibacterial Activity of Silver Nanoparticles Depend on the Shape of the Nanoparticle? A Study of the Gram-Negative Bacterium *Escherichia coli*. *Appl. Environ. Microbiol.* **2007**, *73*, 1712–1720.
13. Ispas, C.; Andreescu, D.; Patel, A.; Goia, D. V.; Andreescu, S.; Wallace, K. N. Toxicity and Developmental Defects of Different Sizes and Shape Nickel Nanoparticles in Zebrafish. *Environ. Sci. Technol.* **2009**, *43*, 6349–6356.
14. Kahru, A.; Dubourguier, H.-C. From Ecotoxicology to Nanoecotoxicology. *Toxicology* **2009**, *269*, 105–119.
15. Evans, D. H.; Piermarini, P. M.; Choe, K. P. The Multifunctional Fish Gill: Dominant Site of Gas Exchange, Osmoregulation, Acid-Base Regulation, and Excretion of Nitrogenous Waste. *Physiol. Rev.* **2005**, *85*, 97–177.
16. Johnston, B. D.; Scown, T. M.; Moger, J.; Cumberland, S. A.; Baalousha, M.; Linge, K.; van Aerle, R.; Jarvis, K.; Lead, J. R.; Tyler, C. R. Bioavailability of Nanoscale Metal Oxides TiO_2, CeO_2, and ZnO to Fish. *Environ. Sci. Technol.* **2010**, *44*, 1144–1151.
17. Scown, T. M.; Santos, E. M.; Johnston, B. D.; Gaiser, B.; Baalousha, M.; Svetlin, M.; Lead, J, R.; Vicki, S.; Fernandes, T. F.; Jepson, M.; et al. Effects of Aqueous Exposure to Silver Nanoparticles of Different Sizes in Rainbow Trout. *Toxicol. Sci.* **2010**, *115*, 521–534.
18. Handy, R. D.; Al-Bairuty, G.; Al-Jubory, A.; Ramsden, C. S.; Boyle, D.; Shaw, B. J.; Henry, T. B. Effects of Manufactured Nanomaterials on Fishes: A Target Organ and Body Systems Physiology Approach. *J. Fish Biol.* **2011**, *79*, 821–853.
19. Hogstrand, C.; Wood, C. M. Toward a Better Understanding of the Bioavailability, Physiology and Toxicity of Silver in Fish: Implications for Water Quality Criteria. *Environ. Toxicol. Chem.* **1998**, *17*, 547–561.
20. Lilius, H.; Sandbacka, M.; Isomaa, B. The Use of Freshly Isolated Gill Epithelial Cells in Toxicity Testing. *Toxicol. In Vitro* **1995**, *9*, 299–305.
21. Aherne, D.; Ledwith, D. M.; Gara, M.; Kelly, J. M. Optical Properties and Growth Aspects of Silver Nanoprisms Produced by a Highly Reproducible and Rapid Synthesis at Room Temperature. *Adv. Funct. Mater.* **2008**, *18*, 2005–2016.
22. George, S.; Pokhrel, S.; Xia, T.; Gilbert, B.; Ji, Z.; Schowalter, M.; Rosenauer, A.; Damoiseaux, R.; Bradley, K. A.; Mädler, L.; et al. Use of a Rapid Cytotoxicity Screening Approach to Engineer a Safer Zinc Oxide Nanoparticle Through Iron Doping. *ACS Nano* **2010**, *4*, 15–29.
23. George, S.; Pokhrel, S.; Ji, Z.; Henderson, B. L.; Xia, T.; Li, L.; Zink, J. I.; Nel, A. E.; Mädler, L. Role of Fe Doping in Tuning the Band Gap of TiO_2 for the Photo-Oxidation-Induced Cytotoxicity Paradigm. *J. Am. Chem. Soc.* **2011**, *133*, 11270–11278.
24. Aruoma, O. I.; Halliwell, B.; Hoey, B. M.; Butler, J. The Antioxidant Action of N-Acetylcysteine: Its Reaction with Hydrogen Peroxide, Hydroxyl Radical, Superoxide, and Hypochlorous Acid. *Free. Radic. Biol. Med.* **1989**, *6*, 593–597.
25. Fubini, B. Surface Reactivity in the Pathogenic Response to Particulates. *Environ. Health Perspect.* **1997**, *105*, 1013–1020.
26. Sayes, C. M.; Reed, K. L.; Warheit, D. B. Assessing Toxicity of Fine and Nanoparticles: Comparing *In Vitro* Measurements to *In Vivo* Pulmonary Toxicity Profiles. *Toxicol. Sci.* **2007**, *97*, 163–180.
27. Lesnykh, N.; Tutukina, N.; Marshakov, I. The Effect of Sulfate and Nitrate Ions on the Passivation and Activation of Silver in Alkaline Solutions. *Protect. Met.* **2008**, *44*, 437–442.
28. Ofek, B.-I.; Ralph, M. A.; Valerie, E. F.; Darin, Y. F. Toxicity Assessments of Multisized Gold and Silver Nanoparticles in Zebrafish Embryos. *Small* **2009**, *5*, 1897–1910.
29. Asharani, P. V.; Wu, Y.; Gong, Z.; Valiyaveettil, S. Toxicity of Silver Nanoparticles in Zebrafish Models. *Nanotechnology* **2008**, *19*, 255102.
30. Xia, T.; Zhao, Y.; Sager, T.; George, S.; Pokhrel, S.; Li, N.; Schoenfeld, D.; Meng, H.; Lin, S.; Wang, X.; et al. Decreased Dissolution of ZnO by Iron Doping Yields Nanoparticles with Reduced Toxicity in the Rodent Lung and Zebrafish Embryos. *ACS Nano* **2011**, *5*, 1223–1235.
31. King-Heiden, T. C.; Wiecinski, P. N.; Mangham, A. N.; Metz, K. M.; Nesbit, D.; Pedersen, J. A.; Hamers, R. J.; Heideman, W.; Peterson, R. E. Quantum Dot Nanotoxicity Assessment Using the Zebrafish Embryo. *Environ. Sci. Technol.* **2009**, *43*, 1605–1611.
32. Choi, J. E.; Kim, S.; Ahn, J. H.; Youn, P.; Kang, J. S.; Park, K.; Yi, J.; Ryu, D.-Y. Induction of Oxidative Stress and Apoptosis by Silver Nanoparticles in the Liver of Adult Zebrafish. *Aquat. Toxicol.* **2010**, *100*, 151–159.
33. Bansal, V.; Li, V.; O'Mullane, A. P.; Bhargava, S. K. Shape Dependent Electrocatalytic Behaviour of Silver Nanoparticles. *Cryst. Eng. Comm.* **2010**, *12*, 4280–4286.
34. Nel, A. E.; Mädler, L.; Velegol, D.; Xia, T.; Hoek, E. M. V.; Somasundaran, P.; Klaessig, F.; Castranova, V.; Thompson, M. Understanding Biophysicochemical Interactions at the Nano-Bio Interface. *Nat. Mater.* **2009**, *8*, 543–557.
35. Ercal, N.; Gurer-Orhan, H.; Aykin-Burns, N. Toxic Metals and Oxidative Stress Part I: Mechanisms Involved in Metal-Induced Oxidative Damage. *Curr. Top. Med. Chem.* **2001**, *1*, 529–539.
36. Zhang, H.; Xia, T.; Meng, H.; Xue, M.; George, S.; Ji, Z.; Wang, X.; Liu, R.; Wang, M.; France, B.; et al. Differential Expression of Syndecan-1 Mediates Cationic Nanoparticle Toxicity in Undifferentiated Versus Differentiated Normal Human Bronchial Epithelial Cells. *ACS Nano* **2011**, *5*, 2756–2769.
37. Meng, H.; Yang, S.; Li, Z.; Xia, T.; Chen, J.; Ji, Z.; Zhang, H.; Wang, X.; Lin, S.; Huang, C.; et al. Aspect Ratio Determines the Quantity of Mesoporous Silica Nanoparticle Uptake by a Small GTPase-Dependent Macropinocytosis Mechanism. *ACS Nano* **2011**, *5*, 4434–4447.
38. Wang, X.; Xia, T.; Ntim, S. A.; Ji, Z.; George, S.; Meng, H.; Zhang, H.; Castranova, V.; Mitra, S.; Nel, A. E. Quantitative Techniques for Assessing and Controlling the Dispersion and Biological Effects of Multiwalled Carbon Nanotubes in Mammalian Tissue Culture Cells. *ACS Nano* **2011**, *4*, 7241–7252.
39. Shao, J.; Dabrowski, M. J.; White, C. C.; Kavanagh, T. J.; Gallagher, E. P. Flow Cytometric Analysis of BDE 47 Mediated Injury to Rainbow Trout Gill Epithelial Cells. *Aquat. Toxicol.* **2010**, *97*, 42–50.
40. Warheit, D. B.; Reed, K. L.; Sayes, C. M. A Role for Nanoparticle Surface Reactivity in Facilitating Pulmonary Toxicity and Development of a Base Set of Hazard Assays As a Component of Nanoparticle Risk Management. *Inhal. Toxicol.* **2009**, *21*, 61–67.
41. Rushton, E. K.; Jiang, J.; Leonard, S. S.; Eberly, S.; Castranova, V.; Biswas, P.; Elder, A.; Han, X.; Gelein, R.; Finkelstein, J.; et al. Concept of Assessing Nanoparticle Hazards Considering Nanoparticle Dosemetric and Chemical/Biological Response Metrics. *J. Toxicol. Environ. Health A* **2010**, *73*, 445–461.